

A new extension of the \mathcal{L}_1 adaptive controller to drastically reduce the tracking time lags

Divine Maalouf* Ahmed Chemori* Vincent Creuze*

*LIRMM, Université Montpellier Sud de France (UMSF)-CNRS, 161 rue Ada,
34392 Montpellier, France

Abstract: The \mathcal{L}_1 adaptive control scheme has proven its effectiveness and robustness in various fields thanks to its particular architecture where robustness and adaptation are decoupled. It was though noted that whenever the trajectory is varying, an inherent lag is present compared to other adaptive schemes due to the presence of a filter in the control architecture. To achieve a better tracking, we propose extending the architecture of the \mathcal{L}_1 controller by augmenting it with a control input that could take the form of a nonlinear proportional or a proportional integral term. The extended scheme is validated through simulations via an illustrative example as well as experimental results performed on an underwater vehicle.

1. INTRODUCTION

Controlling nonlinear dynamic systems is a challenging task. Indeed, not being able to determine the behavior of a system especially in presence of varying parameters, makes difficult the design of a suitable controller. For this reason, the idea of online estimating the uncertain or varying parameters from measurements has emerged. Based on these concepts, adaptive control was therefore born. The recently developed \mathcal{L}_1 adaptive controller (Hovakimyan and Cao [2010]) stands out among all other developed adaptive methods in its particular architecture where robustness and adaptation are decoupled. The low pass filter introduced in its structure separates the estimation loop from the control loop. This guarantees a fast adaptation and compensation of the unmodeled dynamics while still preserving the stability of the closed-loop system. With such a novel method, various previously noted failures in adaptive control were revisited (Kharisov and Hovakimyan [2010] and Xargay et al. [2009]). Besides, an extensive study has been made in Rohrs et al. [1982] showing that restrictive assumptions were formulated upon the use of a wide range of adaptive controllers. These schemes were seen to exhibit undesirable frequency characteristics. An enough parameter excitation might be needed to ensure parameter convergence. This excitation phase allowing the parameters to adapt, will reflect into a bad transient behavior on the system. Consequently, in order to avoid such a behavior, the adaptation gain is usually chosen small which would slow down the system's response. The advantage that the \mathcal{L}_1 adaptive controller brings in this regard lies in the fact that the performance of the closed-loop system can be improved by increasing the adaptation gain without degrading the robustness. A zero steady-state tracking error is guaranteed for constant reference inputs. However, similarly to Model Reference Adaptive Control (MRAC), the error is only guaranteed bounded for time varying reference trajectories. A time lag can be noticed with the \mathcal{L}_1 controller due to the presence of a filter in the control loop. A very careful filter design should then be done to compromise between this time lag and the desired performance bounds. In this paper, we propose a nonlinear proportional and a proportional integral augmentation of this controller in order to reduce the observed tracking error.

The architecture of the \mathcal{L}_1 controller will be therefore extended by adding to the filtered input a proportional (or proportional integral) term and then feeding the resultant to the prediction block and to the controlled system. The application tackled in this paper is within the underwater robotics field. The choice of this controller was motivated by the different advantages previously listed. The identification of an underwater vehicle's model parameters is a very cumbersome task. Those parameters are also likely to vary with the operating environment conditions. A fast and robust adaptation is then necessary in order to perform the desired tasks ranging from pipe or hull following to dam inspection or exploration missions. In the literature, different control schemes were proposed in the literature to solve the arising challenges encountered in autonomous control of underwater robots. We find among them robust \mathcal{H}_∞ control (Roche et al. [2011]), predictive control (Steenenson et al. [2012]) and sliding mode control (Pisano and Usai [2004]). Intelligent control methods using reinforcement learning or artificial intelligence have also been proposed such as Chang et al. [2003] and Carreras et al. [2002]. A more detailed overview of the proposed controllers for underwater vehicles can be found in Yildiz et al. [2009]. The application of the \mathcal{L}_1 adaptive controller is very recent in this field. To the best knowledge of the authors, there are only two reported studies done in simulations: the work of Breu and Fossen [2011] for roll parametric resonance in ships and Svendsen et al. [2012] for the control of a marine watercraft. In our previous work (Maalouf et al. [2012]), we designed, for the first time, this controller with real-time experimental results on an underwater vehicle. The presented work was a regulation in depth and pitch. When the reference trajectory was varied later on, a time lag was observed and therefore a good asymptotic tracking was not achieved. This same time lag was also observed in the other two previously cited papers when simulations were performed. In this paper, we propose to add a proportional (or a proportional integral) input to the filtered one and then send the resulting control input to the state prediction block and to the controlled system. We present the improved results obtained in simulation on an illustrative example extracted from Hovakimyan and Cao [2010], and we also give detailed real-time results for depth control on an underwater vehicle. This paper is organized as follows: in the next section we briefly

* The authors would like to thank the Technalia foundation for its support.

recall the \mathcal{L}_1 adaptive controller architecture, the third section shows the main contribution of this paper with a first validation in simulation. The fourth section presents the application of the proposed extended controller on an underwater vehicle in nominal conditions, then with a parameter variation to show the robustness of the controller. In the fifth section, we display the obtained experimental results and finally the paper ends with some concluding remarks.

2. BACKGROUND ON THE \mathcal{L}_1 ADAPTIVE CONTROL SCHEME

The establishment of the framework of the \mathcal{L}_1 adaptive controller lies in the decoupling between the adaptation and the robustness. For that, the architecture of this scheme is constructed of 4 main parts as shown in Fig. 1 to be explained hereafter: *the controlled system, the state predictor, the adaptation phase and the control law* formulated with a low pass filter.

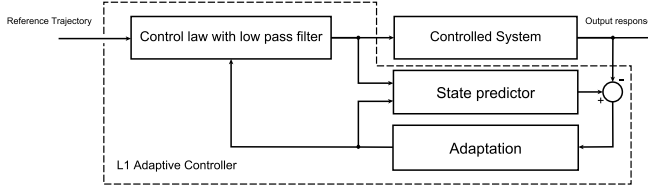


Fig. 1. Block diagram of the \mathcal{L}_1 adaptive controller

- **Controlled System:** We will start by considering the following class of nonlinear systems described by the following dynamics:

$$\begin{aligned} \dot{x}_1(t) &= x_2(t), & x_1(0) &= x_{10} \\ \dot{x}_2(t) &= f(t, x(t)) + B_2 \omega u, & x_2(0) &= x_{20} \\ y(t) &= Cx(t) \end{aligned} \quad (1)$$

where $x_1 \in \mathbb{R}^n$ and $x_2 \in \mathbb{R}^n$ are the states of the system forming the complete state vector: $x(t) = [x_1(t)^T, x_2(t)^T]^T$. $u(t) \in \mathbb{R}^m$ is the control input ($m \leq n$) and $\omega \in \mathbb{R}^{n \times m}$ is the uncertainty on the input gain. $B_2 \in \mathbb{R}^{n \times m}$ is a constant full rank matrix. $C \in \mathbb{R}^{m \times n}$ is a known full rank constant matrix, $y \in \mathbb{R}^m$ is the measured output and $f(t, x(t))$ is an unknown nonlinear function representing the nonlinear dynamics. The partial derivatives of this function with respect to t and to x are assumed to be semi-globally uniformly bounded and $f(t, 0)$ is assumed to be bounded. The previous system of equations can be transformed into a semi-linear one with some assumptions on the boundedness of the parameters and function $f(t, x)$ as described in Cao and Hovakimyan [2008]. It is concluded that this function can be rewritten as:

$f(t, x) = A_2 x_2 + \theta(t) \|x(t)\|_{\mathcal{L}_\infty} + \sigma(t)$ with $\theta(t)$ and $\sigma(t) \in \mathbb{R}^m$ unknown varying parameters. We get the system in matrix form as:

$$\dot{x}(t) = \begin{bmatrix} 0_{n \times n} & \mathbb{I}_{n \times n} \\ 0_{n \times n} & A_2 \end{bmatrix} \begin{bmatrix} x_1 \\ x_2 \end{bmatrix} + \begin{bmatrix} 0_{n \times 1} \\ \theta \end{bmatrix} \|x\|_{\mathcal{L}_\infty} + \begin{bmatrix} 0_{n \times 1} \\ \sigma \end{bmatrix} + \begin{bmatrix} 0_{n \times m} \\ B_2 \end{bmatrix} \omega u \quad (2)$$

$$y(t) = Cx(t)$$

Let $A = \begin{bmatrix} 0_{n \times n} & \mathbb{I}_{n \times n} \\ 0_{n \times n} & A_2 \end{bmatrix}$ be the state matrix describing the actual open-loop system dynamics. It should be modified into a Hurwitz matrix A_m with the desired closed-loop dynamics using a static feedback gain k_m . We would

therefore get $A_m = A - B_m k_m$ with $B_m = \begin{bmatrix} 0_{n \times m} \\ B_2 \end{bmatrix}$. The system can then be finally rewritten in a compact form as:

$$\begin{aligned} \dot{x}(t) &= A_m x(t) + B_m (\omega u_a + \theta(t) \|x(t)\|_{\mathcal{L}_\infty} + \sigma(t)), & x(0) &= x_0 \\ y(t) &= Cx(t) \end{aligned} \quad (3)$$

Given their structure, the vectors θ and σ can be summed to the control input as shown above. In case the matrix B_2 is not an identity matrix, these two uncertain varying parameters would be scaled by the constants contained in B_2 . Since they are unknown, the notation for these two variables will not be changed. u_a is the control input used for adaptation after the transformation of the matrix A into A_m . The whole control input applied to the system is $u = u_m + u_a$ with $u_m = -k_m x$.

- **Adaptation Phase:** This stage uses the error between the measured and the estimated states to update the parameters. The adaptation law for each estimated parameter vector is then given by:

$$\begin{aligned} \dot{\hat{\theta}}(t) &= \Gamma \text{Proj}(\hat{\theta}(t), -(\tilde{x}^T(t) P B_m)^T \|x(t)\|_{\mathcal{L}_\infty}) \\ \dot{\hat{\sigma}}(t) &= \Gamma \text{Proj}(\hat{\sigma}(t), -(\tilde{x}^T(t) P B_m)^T) \\ \dot{\hat{\omega}}(t) &= \Gamma \text{Proj}(\hat{\omega}(t), -(\tilde{x}^T(t) P B_m)^T u_a^T(t)) \end{aligned} \quad (4)$$

The parameter P is the solution to the algebraic Lyapunov equation: $A_m^T P + P A_m = -Q$ for any arbitrary symmetric $Q = Q^T > 0$. Γ is the adaptation gain and $\tilde{x}(t)$ the error between the predicted state and the measured one. The term *Proj* refers to the projection operator which is a robust technique that bounds the estimated parameters by abiding to the Lyapunov stability rules.

- **State Predictor:** The states of the system are calculated at each iteration using the estimated parameters obtained from the adaptation phase (cf. below) along with the control input. Based on equation (3), the state predictor is then given by:

$$\hat{\hat{x}}(t) = A_m \hat{x}(t) + B_m (\hat{\omega}(t) u_a(t) + \hat{\theta}(t) \|x(t)\|_{\mathcal{L}_\infty} + \hat{\sigma}(t)) \quad (5)$$

- **Control law formulation:** The last stage pertains to the formulation of the control input characterized by the addition of a low pass filter. It is written as:

$$u_a(s) = -kD(s)(\hat{\eta}_l(s) - k_g r) \quad (6)$$

$D(s) \in \mathbb{R}^{m \times m}$ is a strictly proper transfer matrix leading to the stable closed-loop filter: $C(s) = \frac{\omega k D(s)}{\mathbb{I}_m + \omega k D(s)}$. k is a positive feedback gain, $k_g = -(C A_m^{-1} B_m)^{-1}$ is a feedforward prefilter to the reference signal $r(t)$ and $\hat{\eta}_l = \hat{\omega}(t) u_a(t) + \hat{\theta} \|x(t)\|_{\mathcal{L}_\infty}$. To ensure the stability of the closed-loop, the feedback gain k and the filter $D(s)$ must be chosen in order to fulfill the \mathcal{L}_1 norm condition. The reader can refer to Hovakimyan and Cao [2010] for the detailed proof of stability.

3. MAIN CONTRIBUTION: EXTENDED \mathcal{L}_1 ADAPTIVE CONTROLLER

The main contribution of this paper lies in the augmentation of the controller presented in the previous section by a nonlinear P/PI feedback as illustrated in Fig.2. The extended section displayed in dotted lines reduces the time lag occurring in presence of a varying reference trajectory when the \mathcal{L}_1 adaptive controller (shown in dashed lines (cf. Fig.2) is employed. Two solutions are proposed here for this added block. A nonlinear proportional integral controller or a proportional integral one

can be used as the additional term to be summed to the original filtered input.

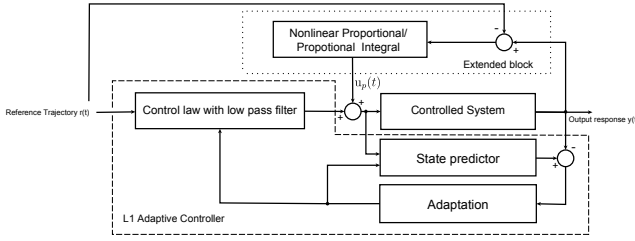


Fig. 2. Block diagram of the extended \mathcal{L}_1 adaptive controller

3.1 Augmentation with a Proportional Integral (PI) controller

For slow dynamical systems, a classical PI could be used to reduce the time lag previously described. In our application, a PI was implemented on an underwater vehicle to improve the closed-loop system performance. The control input $u_p(t)$ shown in Fig. 2 is therefore expressed by:

$$u_p(t) = -K_P e(t) - K_I \int_0^t e(t) dt \quad (7)$$

with K_P and K_I being the proportional and integral gains respectively, and $e(t)$ the tracking error defined by:

$e(t) = y(t) - r(t)$ with $r(t)$ the reference trajectory and $y(t)$ the measured output as shown on Fig. 2.

3.2 Augmentation with a Nonlinear Proportional controller

Conventional PID controllers involve constant gains multiplied by each of the forms of the tracking error (proportional, derivative and integral). For a good trade-off between fast response and reduced overshoot, a nonlinear PID could bring an improvement when the controlled system has a relatively fast dynamics. In our simulation illustrative example, we will refer to the use of a nonlinear proportional since it was enough to reach the desired closed-loop performance.

The added control input $u_p(t)$ can be expressed according to Wang [2012] by the following:

$$u_p(t) = -g(e, \alpha, \delta) \quad (8)$$

with

$$g(e, \alpha, \delta) = \begin{cases} a_1 |e|^\alpha \text{sgn}(e) & \text{if } |e| > \delta \\ a_2 \frac{e}{\delta^{1-\alpha}} & \text{if } |e| \leq \delta \end{cases}$$

where a_1 and a_2 are constant gains (for many applications, it might be preferable to have $a_1 = a_2$ to avoid a discontinuity), e is the tracking error defined in section 3.1, α is a design parameter with $0 < \alpha \leq 1$ and δ is delimiting the transition between the low gains and the high gains. The idea behind this nonlinear proportional term is to have small gains when the error is large and high gains when the error is small.

3.3 Validation in simulation on an illustrative example

The solution with the nonlinear proportional augmentation was applied to the same example given in Hovakimyan and Cao [2010], page 29. In this example, a SISO system is considered. $\sigma = 0$ and ω is a constant with $\omega = 1$. The proposed design parameters are the following: $C(s) = \frac{160}{s+160}$, $\Gamma = 10000$, $k_m = 0$. The closed-loop system is expected to track the following reference trajectory: $r = 100 \cos(0.2t)$. The proportional input considered for the extension of the original controller was designed as

follows:

$$u_p(t) = -g(e, r) \quad (9)$$

with

$$g(e, r) = \begin{cases} 25|e|^{0.1} \text{sgn}(e) & \text{if } |e| > 0.1r \\ 100 \frac{e}{0.1r^{0.9}} & \text{if } |e| \leq 0.1r \end{cases}$$

The obtained simulation results are shown in Fig. 3. The system output is displayed for both versions of the controller. The original \mathcal{L}_1 adaptive controller (dotted blue line) exhibits a clear time lag that becomes insignificant when the proposed proportional extension is added (solid black line). This example illustrates the benefits of extending the original architecture proposed in Hovakimyan and Cao [2010] as explained in this section.

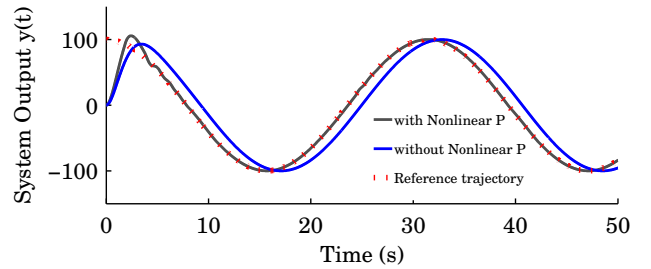


Fig. 3. Performance of the \mathcal{L}_1 adaptive controller: the desired trajectory is displayed in red dashed lines, the \mathcal{L}_1 adaptive controller in blue dotted lines and the proposed extended controller in black solid lines.

4. APPLICATION FOR DEPTH CONTROL OF AN UNDERWATER VEHICLE

4.1 Experimental setup

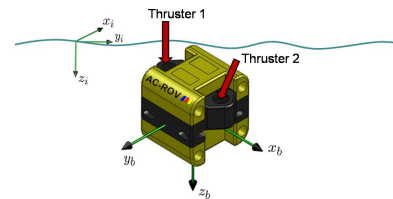


Fig. 4. View of the AC-ROV with the reference frames (x_i, y_i, z_i : earth-fixed frame, x_b, y_b, z_b : body-fixed frame).

The AC-ROV submarine (cf. Fig. 4) is an underactuated underwater vehicle. The propulsion system consists of six thrusters driven by DC motors controlling five degrees of freedom. Four horizontal thrusters control simultaneously translations along x and y axes and rotation around the z axis (yaw angle). The two horizontal thrusters denoted 'Thruster 1' and 'Thruster 2' on Fig. 3 control depth position and pitch angle. The roll angle is unactuated but remains naturally stable due to the relative position of buoyancy and gravity centers. The robot weighs 3 kg and has a rectangular shape with height 203 mm, length 152 mm and width 146 mm. It has been modified by the LIRMM to become computer controllable. The different hardware components of the modified vehicle's hardware are detailed in Maalouf et al. [2012].

The experiments have been performed in a 5 m³ pool. The tether

has been sufficiently deployed to avoid inducing additional drag to the dynamics of the vehicle. The feedback gains have been tuned for the nominal conditions and are kept unchanged for the rest of the experiments despite eventual changes in the model in order to evaluate the robustness of the proposed controller. The experiments were performed for depth control, where the position is measured by a depth sensor whereas the velocity of z direction is estimated by an Alpha-Beta observer (Penoyer [1993]).

4.2 Dynamic modeling of the system

Using the SNAME notation and the representation proposed in Fossen [2002], the depth dynamics of an underwater vehicle, expressed in the body-frame, is given by:

$$M_z \dot{w} + D_z w - \cos(\varphi)\cos(\vartheta)(W - B) = \tau_z + w_{d_z} \quad (10)$$

where \dot{z} and w are the depth velocities in the earth-fixed frame and the body-fixed frame respectively. Due to the coupling in the dynamics, the Euler angles needed for the studied dynamics are the roll (φ) and the pitch (ϑ) expressed in the earth-fixed frame. $J(\varphi, \vartheta) = \cos(\varphi)\cos(\vartheta)$ is the transformation mapping from the body-fixed frame to the earth-fixed one. M_z and D_z denote the inertia (including added mass) and damping respectively. W is the weight and B the buoyancy. w_{d_z} is the term representing the external disturbances and τ_z is the control input expressed in Newton and given by:

$$\tau_z = T K u \quad (11)$$

where $u \in \mathbb{R}^2$ is the vector of control inputs in volts (two thrusters are acting on the degree of freedom of interest, i.e. depth), K is the force coefficient in *Newton.Volt⁻¹* that has been experimentally identified. $T \in \mathbb{R}^{1 \times 2}$ is the actuators configuration matrix taking into account the position and orientation of the propellers, thus allowing to determine the associated forces in the body-fixed frame. Since the chosen reference frame is the earth one, the studied dynamics is then deduced from (10) and transformed into the following:

$$M_z^*(\eta)\dot{\eta} + D_z^*(v, \eta)\dot{\eta} + g_z^*(\eta) = \tau_z^* + w_{d_z}^* \quad (12)$$

The starred terms represent the model terms transformed from the body into the earth frame.

4.3 Implementation of the \mathcal{L}_1 adaptive controller

The original \mathcal{L}_1 adaptive control architecture is applied to the depth z in order to perform a comparison between the two proposed architectures in terms of trajectory tracking and robustness towards uncertainties on the parameters. Rewriting equation (12) in the state space form, we get:

$$\begin{bmatrix} \dot{\eta}_1 \\ \dot{\eta}_2 \end{bmatrix} = \begin{bmatrix} 0 & 1 \\ 0 & \frac{-D_z^*}{M_z^*} \end{bmatrix} \begin{bmatrix} \eta_1 \\ \eta_2 \end{bmatrix} - \begin{bmatrix} 0 \\ \frac{g_z^*}{M_z^*} - \frac{w_{d_z}^*}{M_z^*} \end{bmatrix} + \begin{bmatrix} 0 \\ 1 \\ M_z^* \end{bmatrix} \omega \tau_z^* \quad (13)$$

with $\eta_1 = z$ and $\eta_2 = \dot{z}$. In this case ω is considered to be a constant with $\omega = 1$. Rewriting (13) in the formalism of (3) for the studied dynamics we get:

$$\begin{bmatrix} \dot{\eta}_1 \\ \dot{\eta}_2 \end{bmatrix} = A_m \begin{bmatrix} \eta_1 \\ \eta_2 \end{bmatrix} + \begin{bmatrix} 0 \\ 1 \\ M_z^* \end{bmatrix} (\omega u_a + \theta(t)\|\eta(t)\|_{\mathcal{L}_\infty} + \sigma(t)) \quad (14)$$

$$y = \eta_1 \quad (15)$$

where A_m is obtained from a choice of k_m enabling the state matrix to be Hurwitz, with $A_m \in \mathbb{R}^{2 \times 2}$ and $B_m = [0, \frac{1}{M_z^*}]^T \in \mathbb{R}^{2 \times 1}$. The parameter $\theta \in \mathbb{R}$ represents the uncertainties on the damping

coefficient and is given by: $\theta = \Delta(-D_z^*)$. The parameter $\sigma \in \mathbb{R}$ is a lumped parameter regrouping the gravitational and buoyancy forces as well as the external disturbances $\sigma = -g_z^* + w_{d_z}^*$. The expression $\|\eta(t)\|_{\mathcal{L}_\infty}$ refers to the infinity norm of the state vector at time t . The output is the depth z and the control input is computed in the earth-fixed frame and should be transformed into the body fixed-frame such that: $u = K^{-1}T^{-1}J^T(u_a + u_m) \in \mathbb{R}^2$, with u_a and u_m as explained before.

Remark 1: Given that A_m and B_m are constant matrices, M_z^* and D_z^* in A_2 and B_2 were replaced by M_z and D_z . This will guarantee for A_m a constant desired dynamics. All the uncertainties will be compensated by the controlled parameters $\hat{\theta}$ and $\hat{\sigma}$ that are to be adapted.

4.4 \mathcal{L}_1 adaptive controller augmentation

The controller described in the previous section is compared with the extended one shown in Fig. 2. The control input in this case is expressed by: $u = K^{-1}T^{-1}J^T(u_a + u_m + u_p)$ with u_p given by (7).

5. EXPERIMENTAL RESULTS

In this section the obtained experimental results are presented and discussed. They result from the application of the proposed controllers detailed in section 2 and section 3 to the underwater vehicle described in section 4.1. The aim is to perform a comparison of these two versions of the \mathcal{L}_1 adaptive controller (original and extended) in two scenarios. The obtained results are presented and analyzed in Fig. 5 and 6. The experiments start with the vehicle at the surface (horizontal static position) and it is expected to track a reference trajectory in order to reach different levels of depth.

5.1 Proposed experimental scenarios

Two experimental scenarios were performed, namely:

- i) *Scenario 1:* Control in nominal conditions

The objective of this scenario is to control the depth of the robot without any external disturbance. The gains for each controller have been tuned to accommodate this case and were kept unchanged for the other experiments. The vehicle is expected to track a varying trajectory starting from the surface level to 0.8 m, then 0.4 m and finally 0.6 m.

- ii) *Scenario 2:* Robustness towards a parameter uncertainty
The vehicle was changed by the addition of a piece of polyester introducing a change of buoyancy of +0.2 N which brings a variation of approximately 17% to the parameter $(W - B)$. Such a variation corresponds for instance to the situation where the vehicle encounters a sudden change in the water's salinity. This test of robustness was only applied to the augmented controller given that the \mathcal{L}_1 controller was already proven to be robust to such a change in Maalouf et al. [2012]. The goal of this scenario was to check if the robustness of the \mathcal{L}_1 adaptive controller was not affected by the proposed augmentation.

5.2 Scenario 1: Control in nominal conditions

Figure 5-(a) displays the evolution of the vehicle's position for each of the proposed controllers. The robot is expected to follow a trajectory in z going from the surface and reaching 0.8 m in 40 seconds. After remaining stable at this position for 100 seconds, the vehicle surfaces to 0.4 m in 40 seconds and remains there for 70 seconds before going down to 0.6 m in 60 seconds. The standard \mathcal{L}_1 adaptive controller needs

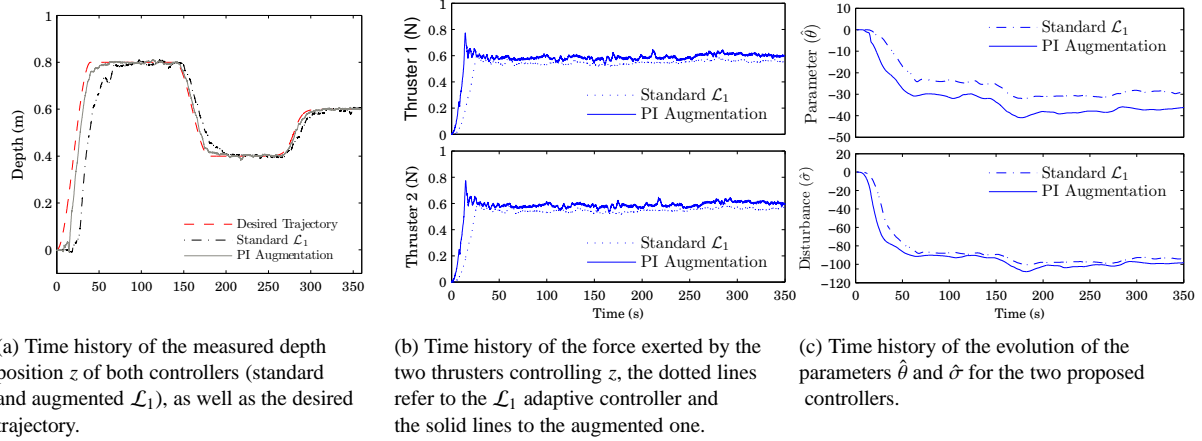


Fig. 5. **Scenario 1: Control in nominal conditions:** for the standard \mathcal{L}_1 adaptive controller (dotted lines) and the augmented one (solid lines), the depth responses are plotted (a), the control inputs (b), and the parameters $\hat{\theta}$ and $\hat{\sigma}$ (c).

around 65 seconds to reach the steady state depth (5% of the final value) with no significant overshoot. The augmented \mathcal{L}_1 adaptive controller reveals to be significantly faster with a convergence in 45 seconds and with no overshoot either. After the convergence to 0.8 cm, a clear time lag is observed when the trajectory was changing with the \mathcal{L}_1 controller while the augmented one is almost able to perfectly track the desired trajectory. We observe that for both controllers we have a smooth response of the thrusters that exert a total force of 1.2 N (cf. Fig. 5-(b)) as well as a parameter convergence (cf. Fig. 5-(c)). The existence of the proportional integral term appears in the control input in Fig. 5-(b) through the steep slope and the noted overshoot. This evolution provided the rapid convergence to the desired trajectory. The estimated parameters were all initialized to zero for both cases and, although the adaptation gains were very high, a smooth convergence is observed. The parameters did not converge to the same values for both controllers since the system did not exhibit the same closed-loop behavior in each case. We conclude from this first scenario that the augmented \mathcal{L}_1 adaptive controller is able to ensure a faster convergence without the necessity of having an *a priori* knowledge of the model parameters. Moreover,

the steady state accuracy is not affected and no overshoot is observed in the output tracking.

5.3 Scenario 2: Robustness towards a parameter uncertainty

The buoyancy added to the system (+0.2 N) disturbs in a persistent way the motion of the vehicle that would tend to float more. On Fig. 6-(a), we observe the overlapped responses of the closed-loop when the augmented \mathcal{L}_1 adaptive controller is applied with and without an added buoyancy. The convergence time in both scenarios is kept unchanged despite this large variation brought on the buoyancy parameter. The explanation behind the absence of any tracking performance degradation lies in the high gains allowing a fast adaptation that guarantees the convergence of the parameters. Consequently one can deduce, that the robustness of the \mathcal{L}_1 controller is still preserved thanks to the control input u_a . In Fig 6-(c), we can see how the parameters converged to different values in order to compensate for the imposed parameter variation without compromising the behavior of the closed loop system. Concerning the control inputs generated for both scenarios, and depicted in Fig. 6-(b), we can observe that the robot's thrusters are exerting more effort when the buoyancy was added in order to immerse the vehicle. We have a combined force of 1.4 N against 1.2 N in the nominal case.

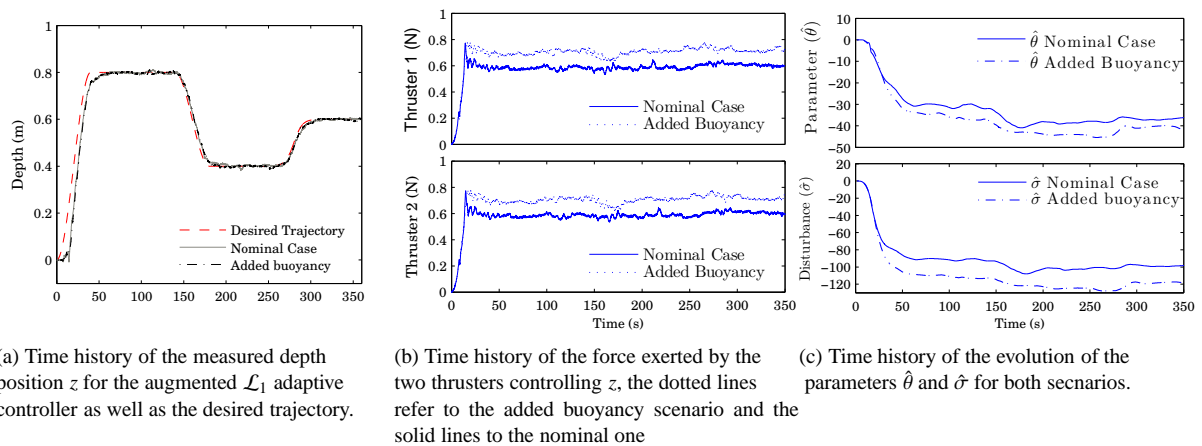


Fig. 6. **Scenario 2: Robustness towards parameter uncertainty:** for the augmented \mathcal{L}_1 adaptive controller, the depth responses are plotted (a), the control inputs (b), and the parameters $\hat{\theta}$ and $\hat{\sigma}$ (c).

5.4 Comparison of the two architectures

Table 1 below summarizes the comparison between the experimental results obtained by both controllers for the nominal case, in terms of settling time and root mean squared error. Table 2 evaluates the robustness of both controllers when the buoyancy parameter is varied. Throughout the performed experiments, it was shown that the augmented \mathcal{L}_1 adaptive controller drove the system faster to the desired state and cancelled the time lag thanks to the added proportional integral term in the control input. The augmented controller was 20 *seconds* faster for the convergence to the first depth level. The Root Mean Squared Error (RMSE) was 3 times smaller than the original \mathcal{L}_1 controller and this RMSE was kept unchanged despite the variation in the buoyancy parameter. All the gains and parameters were identical for both controllers and scenarios, only the added PI input made the difference in the tracking performance of the augmented controller. For the sake of providing a complete comparison between both controllers, the performance of the classical \mathcal{L}_1 adaptive controller is also provided for both scenarios. The experimental results related to the change of buoyancy in the case of the classical \mathcal{L}_1 adaptive controller were not displayed for the sake of space. We observe that the convergence time was almost not affected, however, a more important degradation in terms of the RMSE compared to the augmented controller was noticed.

Table 1. Performance of Both Controllers in the Nominal Case

Nominal Conditions	\mathcal{L}_1 Controller	Augmented \mathcal{L}_1 Controller
Settling Time	65 s	45 s
Root Mean Squared Error	12.1 cm	4.35 cm

Table 2. Performance of the Original and Augmented \mathcal{L}_1 Controller in Both Scenarios

\mathcal{L}_1 Controller	Nominal Case	Change in Buoyancy
Settling Time	65 s	68 s
Root Mean Squared Error	12.1 cm	13.8 cm
Augmented \mathcal{L}_1 Controller	Nominal Case	Change in Buoyancy
Settling Time	45 s	45 s
Root Mean Squared Error	4.35 cm	4.86 cm

6. CONCLUSION

In this paper, the problem tackled was the time lag observed when a system tracks a varying trajectory under an \mathcal{L}_1 adaptive controller. The proposed solution consists in augmenting this controller with a nonlinear proportional or a proportional integral term in order to eliminate the lag and achieve a better asymptotic tracking. The modified architecture was first tested in simulations on an illustrative example previously proposed in literature. It was also validated through real-time experimental results on an underwater vehicle following a varying trajectory in depth. Moreover, this extended version of the \mathcal{L}_1 adaptive controller was also proven to be robust to parameter uncertainties. The future work will include the analysis of stability of the augmented architecture and will provide additional experimental results including the ability of this controller to reject external disturbances in order to validate the performance of the proposed scheme.

REFERENCES

- D.A Breu and T.I Fossen. \mathcal{L}_1 adaptive and extremum seeking control applied to roll parametric resonance in ships. pages 871–876, Proceedings of the 9th IEEE International Conference on Control and Automation (ICCA), Santiago, Chile, December 2011.
- C. Cao and N. Hovakimyan. \mathcal{L}_1 adaptive controller for nonlinear systems in the presence of unmodelled dynamics: Part II, pages 4093–4098, American Control Conference, Seattle, WA, June 2008.
- M. Carreras, J. Yuh, and J J Batlle. High-Level control of autonomous robots using a behavior-based scheme and reinforcement learning. In *15th Triennial World Congress of the International Federation of Automatic Control*, Barcelona, 2002.
- M. Chang, W. Chang, and H.H Liu. Model-based fuzzy modeling and control for autonomous underwater vehicles in the horizontal plane. *Journal of Marine Sciences and Technology*, 11:155–163, 2003.
- T.I Fossen. *Marine Control Systems: Guidance, Navigation and Control of Ships, Rigs and Underwater Vehicles*. Marine Cybernetics, As,Trondheim, 2002.
- N. Hovakimyan and C. Cao. *\mathcal{L}_1 Adaptive Control Theory*. Society of Industrial and Applied Mathematics, 2010.
- E. Kharisov and N. Hovakimyan. Comparison of several adaptive controllers according to their robustness metrics. Guidance, Navigation and Control Conference, Toronto, 2010.
- D. Maalouf, V. Creuze, and A. Chemori. A novel application of multivariable \mathcal{L}_1 adaptive control: From design to real-time implementation on an underwater vehicle. In *IEEE/RSJ IROS'12*, Algarve, Portugal, 2012.
- A. Pisano and E. Usai. Output-feedback control of an underwater vehicle prototype by higher-order sliding modes. *Automatica*, 40(9):1525–1531, 2004.
- E. Roche, O. Senname, D. Simon, and S. Varrier. A hierarchical varying sampling \mathcal{H}_∞ control of an auv. In *18th IFAC world congress*, Milano, Italy, 2011.
- C.E Rohrs, L. Valavani, M. Athans, and G. Stein. Stability problems of adaptive control algorithms in the presence of unmodeled dynamics. 21st Conference on Decision and Control, Orlando,FL, December 1982..
- R. Penoyer. The alpha-beta filter. *C User's Journal*, 11(7): 73–86, 1993.
- L.V. Steenson, A.B. Phillips, E. Rogers, M.E. Furlong, and S.R. Turnock. Experimental verification of a depth controller using model predictive control with constraints onboard a thruster actuated auv. IFAC Workshop on Navigation, Guidance and Control of Underwater Vehicles (NGCUV2012), Ireland, April 2012..
- C.H. Svendsen, N.O Holck, R. Galeazzi, and M. Blanke. \mathcal{L}_1 adaptive manoeuvring control of unmanned high-speed water craft. Proceedings of the 9th IFAC Conference on Manoeuvring and Control of Marine Crafts, Arenzano, Italy, September 2012.
- W. Wang. *PID Controller Design Approaches - Theory, Tuning and Application to Frontier Areas*. InTech, 2012.
- E. Xargay, N. Hovakimyan, and C. Cao. Benchmark problems of adaptive control revisited by \mathcal{L}_1 adaptive control. pages 31 – 36, 17th Mediterranean Conference on Control and Automation, Thessaloniki, June 2009.
- O. Yildiz, A.E. Yilma, and B. Gokalp. State-of-the-Art System Solutions for Unmanned Underwater Vehicles. *Radioengineering*, 18(4):590–600, 2009.